

Composition-Dependent Long-Term Stability of Mosaic Solid-Electrolyte Interface for Long-Life Lithium-Ion Battery

Vallabha Rao Rikka,^[a, b] Sumit Ranjan Sahu,^[a] Abhijit Chatterjee,^[b] R. Gopalan,^[a] G. Sundararajan,^[a] and Raju Prakash^{*[a]}

The solid-electrolyte interface (SEI) layer determines the fast charging capability and cycle life of a lithium-ion battery. In-depth investigation of the mosaic SEI layer's formation, growth, and stability are of utmost importance to obtain a stable electrochemical performance over cycles. We investigate the stability of the mosaic SEI layer during cycling at a high C-rate (0.5 C). The composition of the SEI layer is governed by the current density-dependent formation of inorganic and organic

compounds. The inorganic compounds rich outer SEI layer and organic compounds rich inner SEI layer formed after the first lithiation helps in preventing SEI breakdown and growth during cycling. The SEI layer densifies during cycling as a result of the decomposition of the entrapped electrolyte. The composition-dependent stability of the mosaic SEI layer stability opens up new possibilities for extending the cycle life of lithium-ion batteries.

1. Introduction

Lithium-ion batteries (LIBs) have emerged as important energy storage solutions for stationary, portable electronics, and electric vehicle applications.^[1] Performance, cycle life, fast charging, and safety are the key disruptors in escalating the market size of LIBs.^[2] Graphite is the most commonly used anode material in LIBs due to its low potential, low cost, and excellent structural stability.^[3] During the first charge, a thin passivation layer forms on the graphite anode due to the electrochemical reduction of electrolyte, referred to as a solid electrolyte interface (SEI) layer.^[4] This causes loss of lithium inventory (LLI) which is undesirable but inevitable.^[5] The SEI layer is an electronic insulator; it ceases further reduction of the electrolyte and co-intercalates solvated molecules into graphite layers in subsequent discharge cycles.^[5]

The formation of a uniform and stable SEI layer within few cycles is challenging and depends on several factors such as C-rate, cell temperature, and the chemical composition of the SEI layer.^[5–7] Usually, low C-rates (0.05–0.1 C) and ambient temperature (23–40 °C) helps in forming a uniform and thin SEI layer on the anode surface.^[5] On the other hand, the volume change of graphite during lithiation/de-lithiation is typically 13%, which might fracture the SEI layer during repeated cycling

resulting in active lithium-ion loss.^[6–7] The stability of the SEI layer is an important aspect of cell performance^[6] as an unstable and non-uniform SEI layer might lead to undesirable loss of reversible lithium ions during charge-discharge cycles due to SEI breakdown-reformation and shorten the cycle life of the cell. In a cell, due to the limited active lithium loading on the cathode, the cycle life of the lithium-ion cell is directly proportional to the loss of reversible lithium ions. Therefore, a stable SEI layer with an optimum thickness, composition, and electrical resistance is beneficial for the fast-charging capability, long life, and safety of LIB. To date, the structure and chemical composition of the SEI layer has been reported to be dependent on the salt, solvent, and additives present in the electrolyte, but under extreme battery operating conditions, including high voltage window, high C-rate, and high temperature (>40 °C), the SEI suffers from inferior stability.^[8–10] Therefore, more comprehensive research on this topic is required to improve the stability of the SEI layer.

The stability of the SEI layer is governed by the ratio of organic-to-inorganic compounds formed,^[11] which leads to good capacity retention. It is important to understand whether the high concentration of inorganic or the organic compounds is more important to the SEI stability and capacity retention. In general, the inorganic compounds (LiF, Li₂O, and Li₂CO₃) formed in the SEI layer are less soluble in the electrolyte as compared to the organic compounds (ROLi, RCOOLi, and ROCOOLi), due to its high heat of salt dissolution, which helps in the formation of a dense SEI layer.^[12] While the organic compounds being porous, helps in better percolation of electrolyte and enhances the lithium-ion conduction.^[12] There are a number of proposed models on SEI formation, such as multilayer, mosaic and mixed multilayer-mosaic.^[13–15] The mosaic SEI layer was formed as a result of the decomposition of the various electrolyte components (salt, additives and solvents) at various electrochemical potentials and simultaneous deposition of organic and inorganic compounds on the graph-

[a] V. Rao Rikka, Dr. S. Ranjan Sahu, Dr. R. Gopalan, Prof. G. Sundararajan, Dr. R. Prakash
Centre for Automotive Energy Materials
International Advanced Research Centre for Powder Metallurgy and New Materials (ARCI)
Chennai 600113, Tamil Nadu, India
E-mail: rprakash@arci.res.in

[b] V. Rao Rikka, Prof. A. Chatterjee
Department of Chemical Engineering
Indian Institute of Technology Bombay
Powai 400076, Maharashtra, India

 Supporting information for this article is available on the WWW under
<https://doi.org/10.1002/batt.202100127>

ite surface to form polyhetero microphases. Recently, the well-accepted mosaic SEI layer has been experimentally demonstrated for the first time, where the formation and growth mechanisms (~ 150 nm thickness) were studied as a function of different discharge voltages⁴. However, the stability of a mosaic SEI layer under high C-rate cycling is not well understood. It is widely accepted that the inorganic-rich inner SEI layer is more prone to cracking due to volume changes in the electrode during charge-discharge cycles.^[12,16] This leads to LLI and poor cycling stability of the graphite anode.

In the present work, we have studied the stability of the mosaic SEI layer during cycling (20 cycles) at 0.5 C. It was observed that the thickness of the SEI layer formed after the first lithiation was almost unchanged during cycling. The outer SEI layer formed after the first lithiation at low C-rate was found to be rich in inorganic compounds, which provided stability to the SEI layer during cycling and ensured good capacity retention. After cycling, the amount of inorganic and organic compounds was almost comparable, which is a characteristic of a stable SEI layer. The current density dependent change in the chemical composition of the SEI layer was studied. Besides, a comprehensive study on the morphological features and impedance of the SEI layer was performed after the first and 20 charge-discharge cycles, which facilitated in understanding the chemical composition dependent stability of the SEI layer.

2. Results and Discussion

2.1. Formation of SEI Layer and Electrochemical Cycling of Graphite Anode

The first lithiation and delithiation of the graphite were carried out at 0.05 C (Figure 1a). The initial cycle irreversible capacity loss (ICL) of 53 mAh g^{-1} could be ascribed to the SEI layer formation. The formation of the SEI layer comprises nucleation, deposition, growth, and densification stages (Scheme 1).^[4,17] Initially, due to the electrolyte decomposition, the SEI compounds nucleate in the electrolyte at $\sim 1.8 \text{ V}$ (Scheme 1a). Once the nuclei concentration in the electrolyte reaches supersaturation ($\sim 0.75 \text{ V}$), the nuclei deposit on the graphite surface as islands (Scheme 1b). The islands join together to form a porous SEI layer (Scheme 1c), which partially covers graphite surfaces. The continuous growth of the SEI layer takes place up to $\sim 0.12 \text{ V}$ as more SEI compounds deposit on the graphite (Scheme 1d). Finally, a mosaic SEI layer composed of a mixture of inorganic and organic compounds is formed (Scheme 1e) after lithiation at $\sim 0.05 \text{ V}$.^[4] Subsequently, the graphite was cycled at 0.5 C over 20 cycles. The charge-discharge curves are shown in Figure 1b.

The first cycle lithiation and delithiation capacities were found to be 318 and 314 mAh g^{-1} (Figure 1c). The lithiation

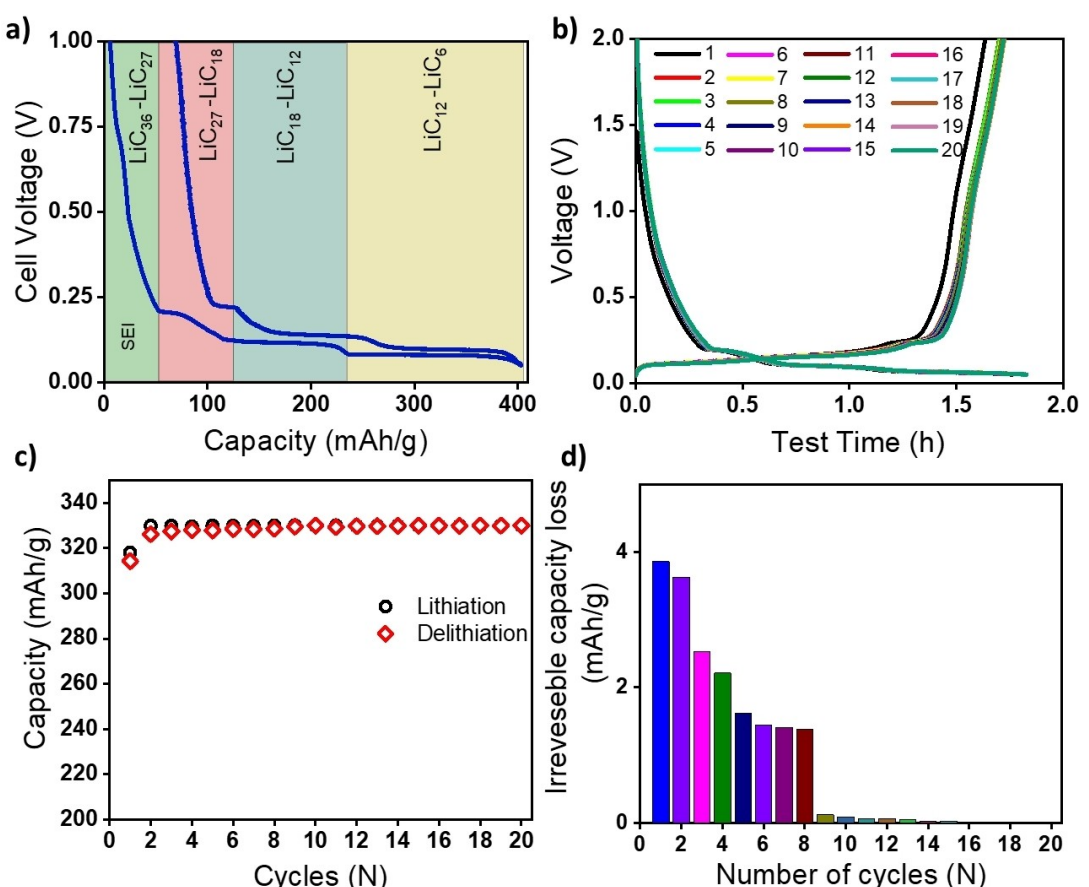
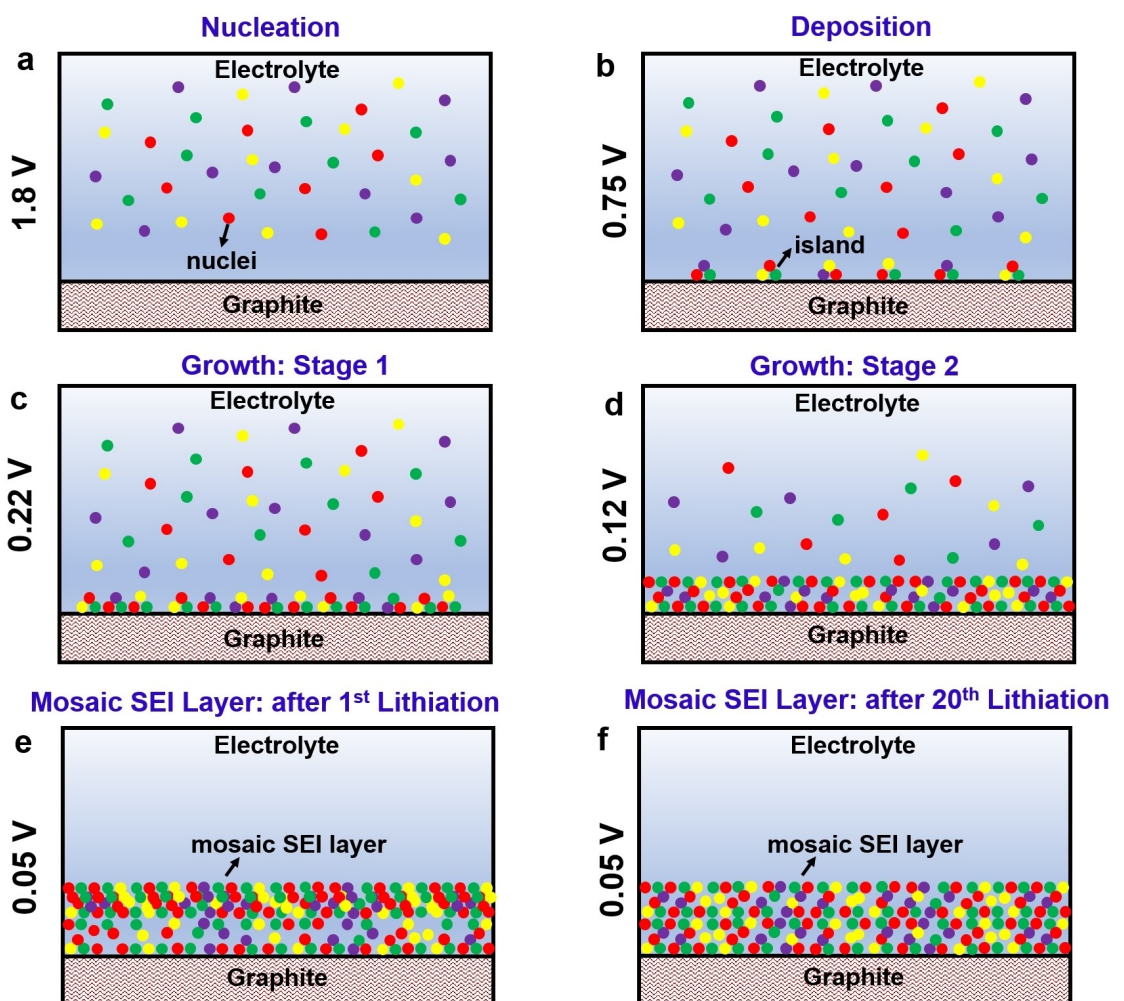


Figure 1. Electrochemical performance of graphite anode. a) 1st Charge-discharge cycle at 0.05 C; b) charge-discharge cycles at 0.5 C; c) lithiation-delithiation capacity at 0.5 C vs. cycle number, and d) irreversible capacity loss vs. cycle number.



Scheme 1. The mosaic SEI layer formation. a) Nucleation; b) deposition; c, d) growth; e) SEI layer after 1st lithiation, and f) SEI layer after 20th lithiation.

capacity was almost constant from the second cycle onwards, whereas the delithiation capacity increased over the cycles, which could be due to the densification of the SEI layer during cycling. The ICL was calculated for each cycle and plotted against the cycle number (Figure 1d). A Coulombic efficiency of ~100% was achieved from the ninth cycle, which indicates that a stable SEI layer was obtained after nine cycles. However, the charge-discharge cycles were continued up to 20 cycles to determine the stability of the SEI layer. After the 20th lithiation more stable SEI layer was confirmed on the graphite surface (Scheme 1f).

2.2. TEM Analysis of SEI Layer

Figure 2a shows the TEM image of the fresh graphite surface before cycling. After 1st lithiation, a uniform mosaic SEI layer with a thickness of ~150 nm was observed on the graphite surface (Figure 2b). The inner SEI layer (75 nm) appears dark and porous, possibly resulting from the more organic compound formation. While the relatively brighter appearance of the outer SEI layer (~75 nm) can be accredited to the dense

inorganic compounds. The SEI layer thickness was almost unaltered (~150 nm) after cycling (Figure 2c), but it appears to be denser and more homogenous in composition as compared to that after 1st lithiation. The selected area electron diffraction (SAED) pattern of the SEI layer revealed bright diffraction spots (Figure 2d) for Li₂CO₃ (31-1), Li₂O (002), and LiF. (111). The *d*-spacing was calculated to be 0.24, 0.23, and 0.22 nm, respectively.

2.3 Structure and Composition of the Mosaic SEI Layer

The structure and composition of the mosaic SEI layer formed after the 20th lithiation were examined by X-ray photoelectron spectroscopy (XPS) analysis. Figure 3 shows the XPS depth profile spectra of graphite electrodes after 20 cycles with respect to different sputtering times (0, 2, 5, and 8 minutes). A higher sputtering time implies that the SEI layer is closer to the surface of the graphite particle. The inorganic compounds (LiF, Li₂O, and Li₂CO₃) and the organic compounds (ROCOOLi, RCOOLi, and ROLi) were identified with corresponding binding energies in the O 1s, Li 1s, C 1s, and F 1s spectrum (Figure 3a–

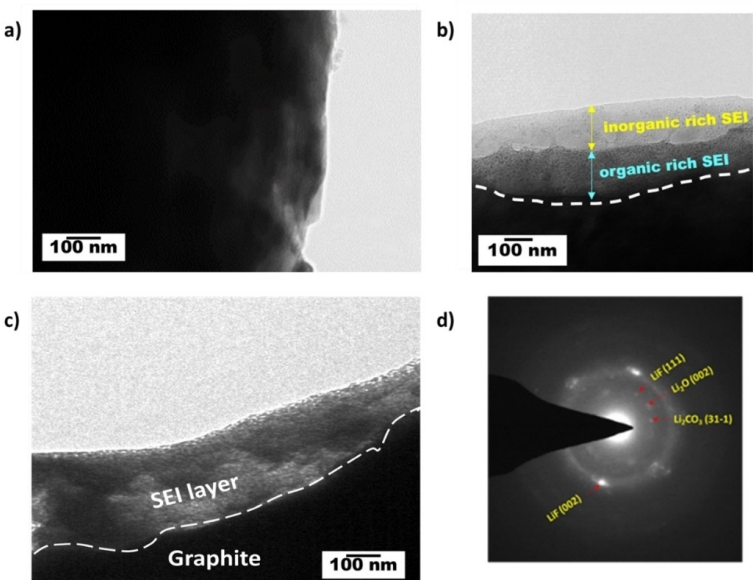


Figure 2. TEM images. a) Fresh graphite surface; b) SEI layer after 1st lithiation; c) SEI layer after 20th lithiation, and d) corresponding SAED pattern.

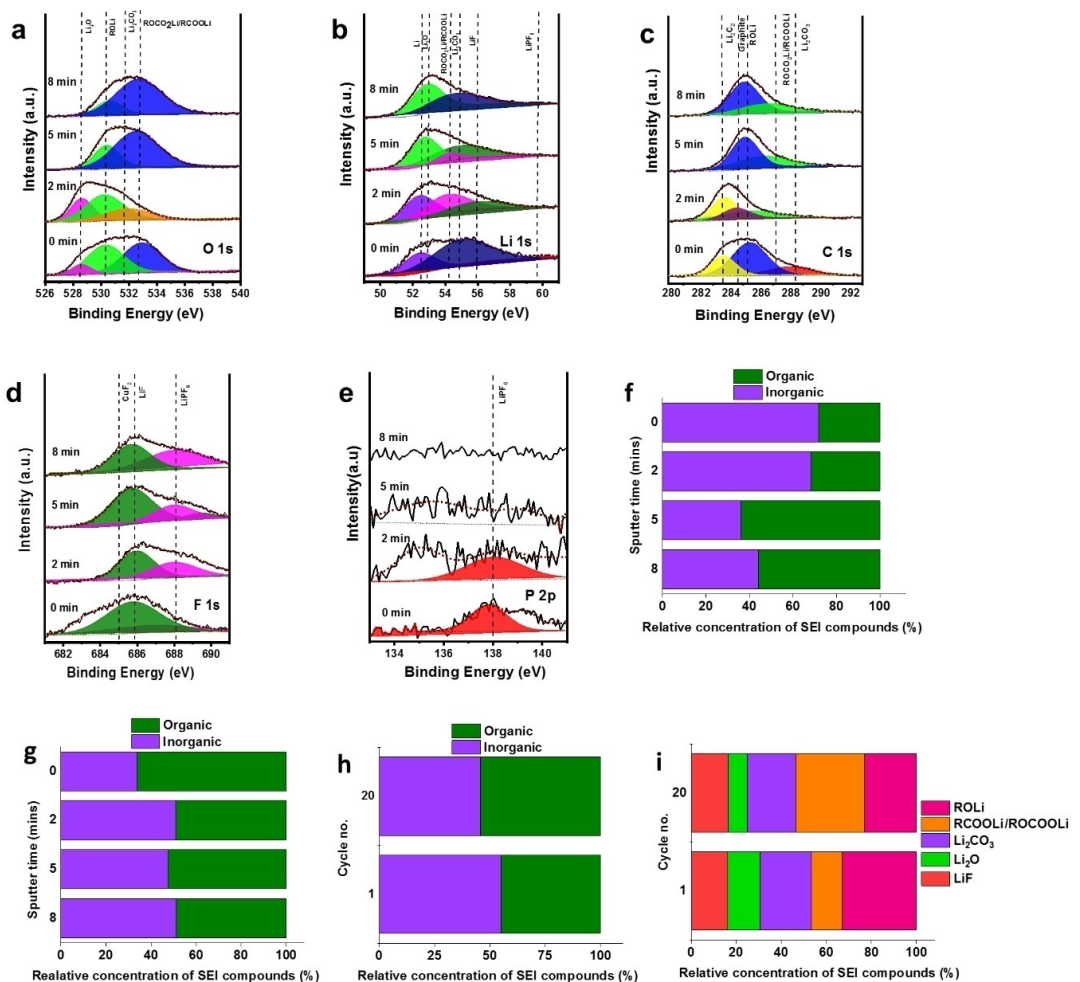


Figure 3. XPS spectrum of the mosaic SEI layer after 20th lithiation after different sputtering times. a) O 1s; b) Li 1s; c) C 1s; d) F 1s; e) P 2p; f) relative concentration of SEI compounds after 1st lithiation; g) relative concentration of SEI compounds after 20th lithiation; h) comparison of total inorganic-to-organic compounds after 1st and 20th lithiation and i) comparison of the relative concentrations of various organic and inorganic compounds in the mosaic SEI layer after 1st and 20th lithiation.

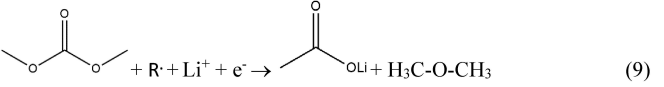
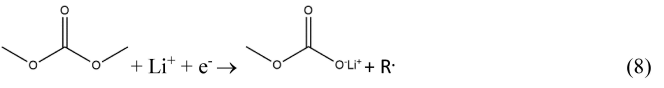
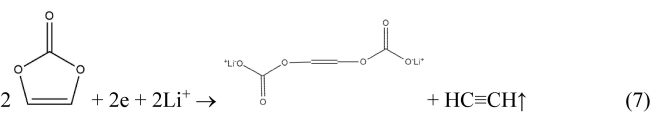
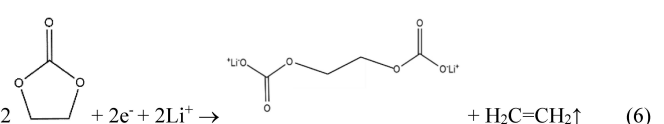
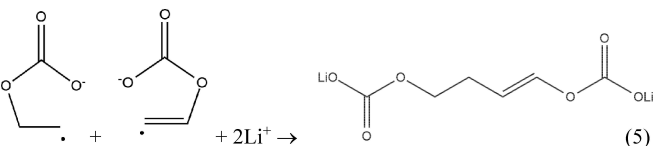
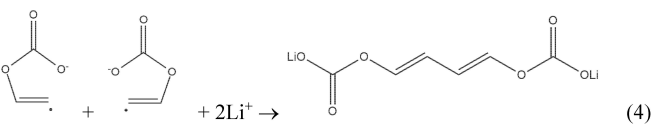
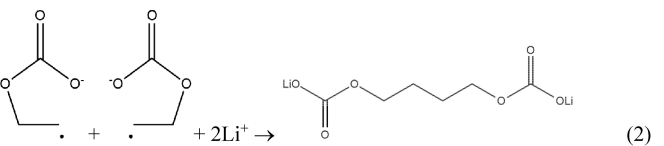
d, Table S1).⁴ Presence of a small amount of undissociated LiPF₆ (corresponding to the peak ~137.3 eV in the P 2p spectra)^[4] has also been identified towards the outer mosaic SEI layer (Figure 3e). After peak fitting, the relative concentrations of the various chemical compounds in the SEI layer were calculated using the equation $C = (I_x/S_x)/(\sum I_i/S_i)$, where I_x and S_i denote the relative intensity and sensitivity number of the compound, respectively.^[18] The relative amount of the inorganic and organic compounds with reference to depth of the SEI layer is shown in Figure 3f (for 1st cycle) and Figure 3g (for 20th cycle). The relative amount of the organic and inorganic compounds after 1st lithiation was calculated from the XPS data reported in our previous work.^[4] The coexistence of the organic and inorganic compounds at various depths (different sputtering times) of the SEI layer provides evidence towards the formation of a mosaic SEI layer. After 1st lithiation, the outer part of the SEI layer was rich in inorganic compounds, while the inner part of the SEI layer was mostly composed of organic compounds (Figure 3f). This is a new observation with respect to the earlier reports where it was perceived that the amount of inorganic compounds would be relatively higher towards the inner SEI layer.^[12,19–21]

This type of structure of the mosaic SEI layer could have prevented the breakdown and reformation of the mosaic SEI layer during cycling at a high C-rate. As the graphite undergoes ~13% volume change during lithiation/delithiation,^[22] the organic compounds rich flexible inner SEI layer at the vicinity of the graphite surface, could efficiently accommodate the stress generated on the SEI layer during initial cycles.^[18,22,23] The inorganic compounds rich outer SEI layer, due to its electron insulating property, effectively reduced the rate of the electrolyte reduction on the surface of the graphite and prevented the rapid SEI growth during cycling. After the 20th lithiation, the relative concentration of the organic compounds increases towards the outer mosaic SEI layer (Figure 3g). In contrast, the inorganic compound concentration was increased in the inner SEI layer. The total inorganic-organic compound ratio of the mosaic SEI layer was close to 1:1 after 1st and 20th lithiation (Figure 3h), which could have provided adequate mechanical strength and flexibility to the SEI layer for stable electrochemical cycling (Figure 1b) at 0.5 C.

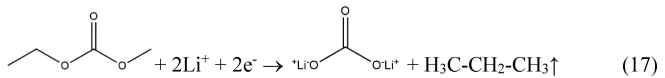
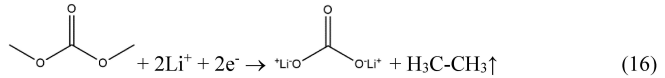
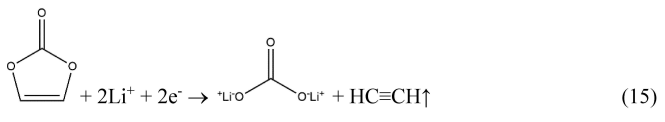
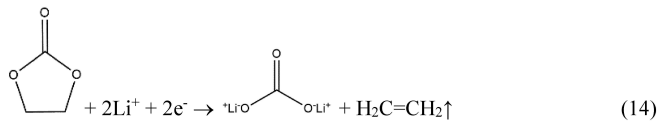
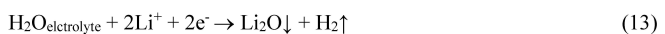
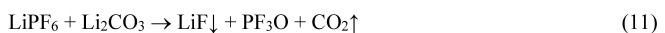
2.4. Formation Mechanism of the Mosaic SEI Layer

The formation of the mosaic SEI layer occurs in two steps. Initially, the electrons are transferred from the surface of the current collector to the graphite. Simultaneously the solvated lithium ions reach the surface of the graphite and get reduced by the electrons.^[24] Therefore, the applied current rate has a significant effect on the rate of formation of the SEI compounds via one- and two-electron reduction pathways.^[12,24] The plausible reaction pathways for the formation of the SEI compounds are listed below.^[4,5,25]

2.4.1. One Electron Reduction: Formation of Oligomers and Organic Compounds



2.4.2. Two Electron Reduction: Formation of Inorganic Compounds



The relative concentrations of chemical compounds in the mosaic SEI layer after the first lithiation were estimated from the XPS peak-area analysis and compared to the 20th lithiation (Figure 3i). The change in the relative concentration of the SEI layer compounds after cycling indicates a difference in the rate of the formation of the compounds during cycling. Generally, the organic compounds ROLi, RCOOLi, ROCooli, and oligomers ($\text{C}_2\text{H}_2\text{OCO}_2\text{Li}$)₂, ($\text{C}_2\text{H}_4\text{OCO}_2\text{Li}$)₂, ($\text{C}_2\text{H}_3\text{OCO}_2\text{Li}$)₂, Li₂EDC ($\text{CH}_2\text{OCO}_2\text{Li}$)₂, and Li₂VDC (CHOCO_2Li)₂ form via a one-electron reduction mechanism, while the inorganic compounds (LiF, Li₂O, Li₂CO₃) form via two-electron reduction pathway. The rate of formation of RCOOLi and ROCooli was found to be the highest during cycling as it involves radical generation (R). Each R· radical generated during the formation of ROCooli [Eq. (8)] leads to the formation of one RCOOLi [Eq. (9)]. While the rate of the formation of Li₂O was the lowest among all after the 20th lithiation, as most of the moisture present in the electrolyte was decomposed to Li₂O during the 1st lithiation [Eq. (13)].

The SEI layer is electrically insulated, and the number of electrons reaching the surface of the graphite particle is governed by the current density.^[24] During 1st lithiation, as the applied current density is relatively low (0.05 C), the rate of the formation of the organic compounds (involving one-electron reduction) via Equations (1)–(10) becomes more feasible at the vicinity of the graphite surface as evident from the XPS analysis (Figure 3f). Besides, due to the fast polymerization rate of vinylene carbonate (VC) and ethylene carbonate (EC) radicals, the oligomers form at greater proportion near the graphite surface,^[25] which increases organic compound concentration within the inner SEI layer. On the other hand, the formation of the inorganic compounds via a two-electron reduction reaction [Eqs. (11)–(17)] occurs towards the outer SEI layer with higher feasibility. Although the current density is relatively low during the 1st lithiation, the rate of formation of the inorganic compounds is driven towards the forward direction due to the

presence of the surplus amount of solvents, for example, ethyl methyl carbonate (EMC), ethylene carbonate (EC), dimethyl carbonate (DMC), vinylene carbonate (VC) additive, LiPF₆ salt, H₂O molecules, and Li⁺ ions near the shore of the electrolyte.

The surplus amount of reactants shifts the reaction equilibrium towards the right-hand side [Eqs. (11)–(17)]. Hence, after the 1st cycle, inorganic compounds in the outer SEI layers are relatively higher than organic compounds. (Figure 3f). A ten times higher current density (0.5 C) is applied on the graphite electrode during cycling compared to the 1st lithiation (0.05 C). The electrolyte present in the porous inner SEI layer undergoes a two-electron reduction reaction with higher feasibility resulting in more inorganic compounds. Meanwhile, towards the outer mosaic SEI layer, which is relatively compact due to more inorganic compounds, undergoes electrolyte decomposition through radicals (involving one electron).^[25] The radical-mediated electrolyte decomposition leads to the formation of oligomers and organic compounds, increasing the concentration of the organic compound in the outer mosaic SEI layer (Figure 3g).^[26]

The XPS analysis shows that a chemical change occurred in the mosaic SEI layer during cycling. This was also supported by charge-discharge cycling data (Figure 1c), where a stable delithiation capacity was observed from the ninth cycle onwards. Herein, we propose a “sponge model” of the mosaic SEI layer to explain the observation. The mosaic SEI layer formed after 1st lithiation (~150 nm thick) is porous and flexible and could be considered as a “sponge” (Figure 4a). After 1st delithiation, the volume of the graphite contracts by 13% and the SEI layer undergoes stress relaxation.^[22] During this process, the electrolyte gets entrapped inside the pores of the sponge SEI layer (Figure 4b). The total LLI due to the SEI formation and electrolyte entrapment gets reflected in the first cycle irreversible loss in the cycling data (Figure 1c). During cycling, the entrapped electrolyte undergoes radical assisted decomposition to form more SEI compounds^[27] (Figure 4c), as evident from the increase in the Coulombic efficiency (Figure 1c). After 20th lithiation, a compact and dense mosaic SEI layer forms on the graphite surface without any change in the thickness (Figure 4d).

2.5. Microstructure of the Mosaic SEI Layer

The morphology of the mosaic SEI layer formed after 1st and 20th lithiation was studied via SEM. The fresh graphite particles on the TEM grid are shown in Figure 5a. After the 20th lithiation, the graphite particles are uniformly covered with the SEI layer (Figure 5b). The fresh graphite particle before lithiation showed a smooth surface (Figure 5c). After 1st lithiation, the graphite surface was uniformly covered by the SEI layer (Figure 5d). After the 20th lithiation, the SEI layer on the graphite surface becomes more compact and denser (Figure 5e).

The high magnification images of the SEI layer after 1st lithiation revealed various morphological features present randomly over the entire SEI region (Figure 6a–o). The porous region consists of granular particles (~200 nm) (Figure 6a) and

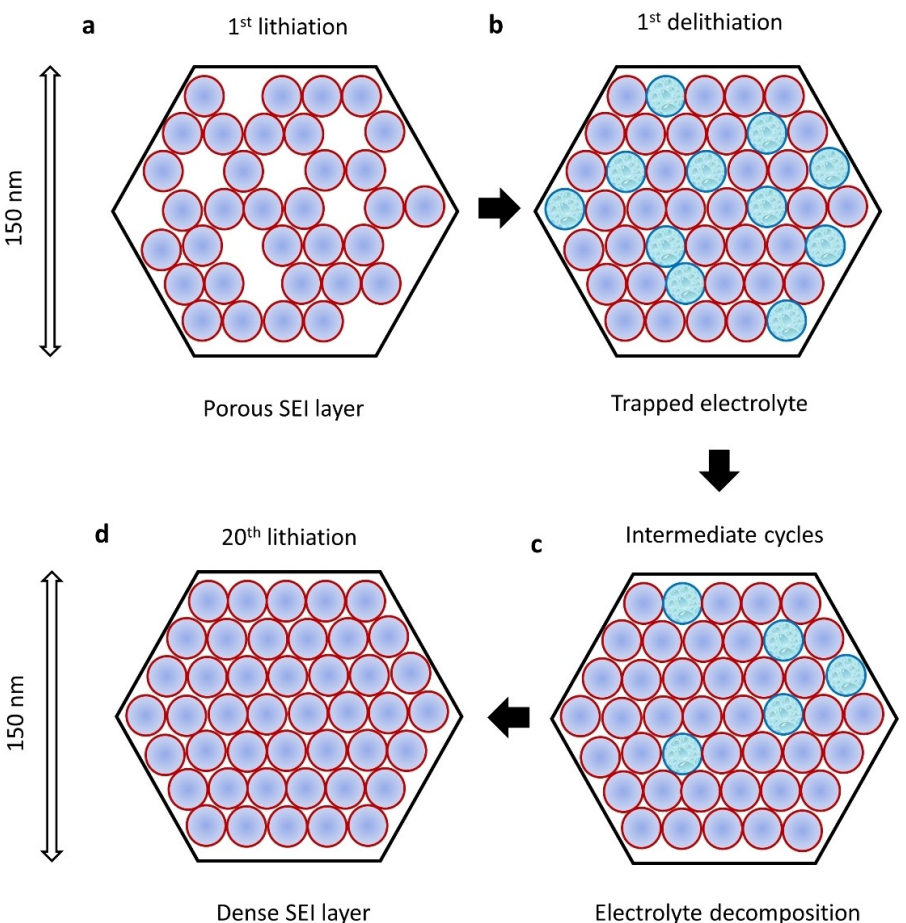


Figure 4. The “sponge model” of the mosaic SEI layer. a) After 1st lithiation; b) after 1st delithiation; c) intermediate cycles, and d) after 20th lithiation.

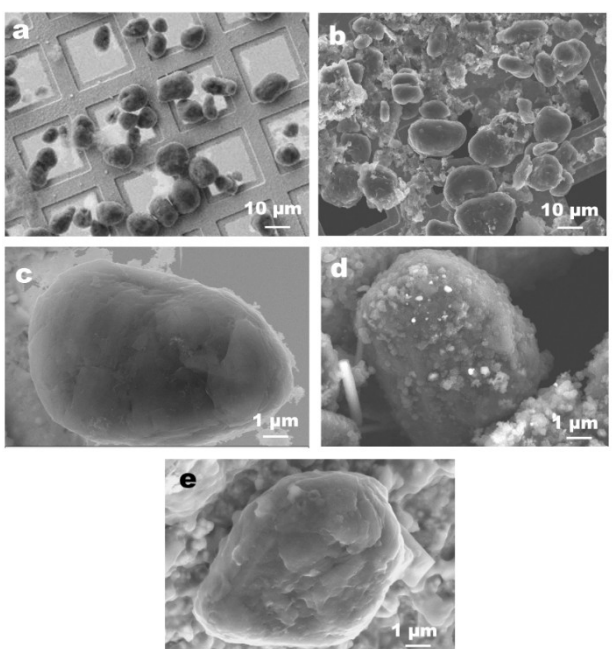


Figure 5. Graphite particles on a TEM grid a) before cycling; b) after 20th lithiation; c) fresh graphite particle; d) graphite particle after 1st lithiation, and e) graphite particle after 20th lithiation.

rod-like structures (Figure 6d). The corresponding energy dispersive X-ray (EDX) mapping data exhibited that they are rich in fluorine (Figure 6b, e) which could be ascribed to inorganic compound LiF. The compact region of the SEI layer was mostly covered with fine needle-like microstructures (Figure 6g), which are rich in oxygen and carbon. In a few areas, corn-like (Figure 6j) and bead-like morphologies (Figure 6m) were also observed to be rich in oxygen and carbon. The oxygen and carbon-rich regions can be assigned to organic compounds Li_2CO_3 , ROLi, RCOOLi, ROCOOOLi, and oligomers (Li_2EDC , Li_2VDC).

After the 20th lithiation, the EDX elemental mapping on the SEI-covered graphite particle (Figure 7a) displayed the uniform distribution of carbon, oxygen, and fluorine (Figure 7b-d). Based on this observation, it is evident that the inorganic and organic compounds are distributed uniformly on the graphite particles. Figure 7e shows the porous nature of the mosaic SEI layer, which could be due to a higher concentration of the organic compounds in the outer mosaic SEI layer, as evident from the XPS analysis (Figure 3g). The corresponding elemental mapping (Figure 7f-h) showed uniform distribution of organic and inorganic compounds on the top surface of the mosaic SEI layer.

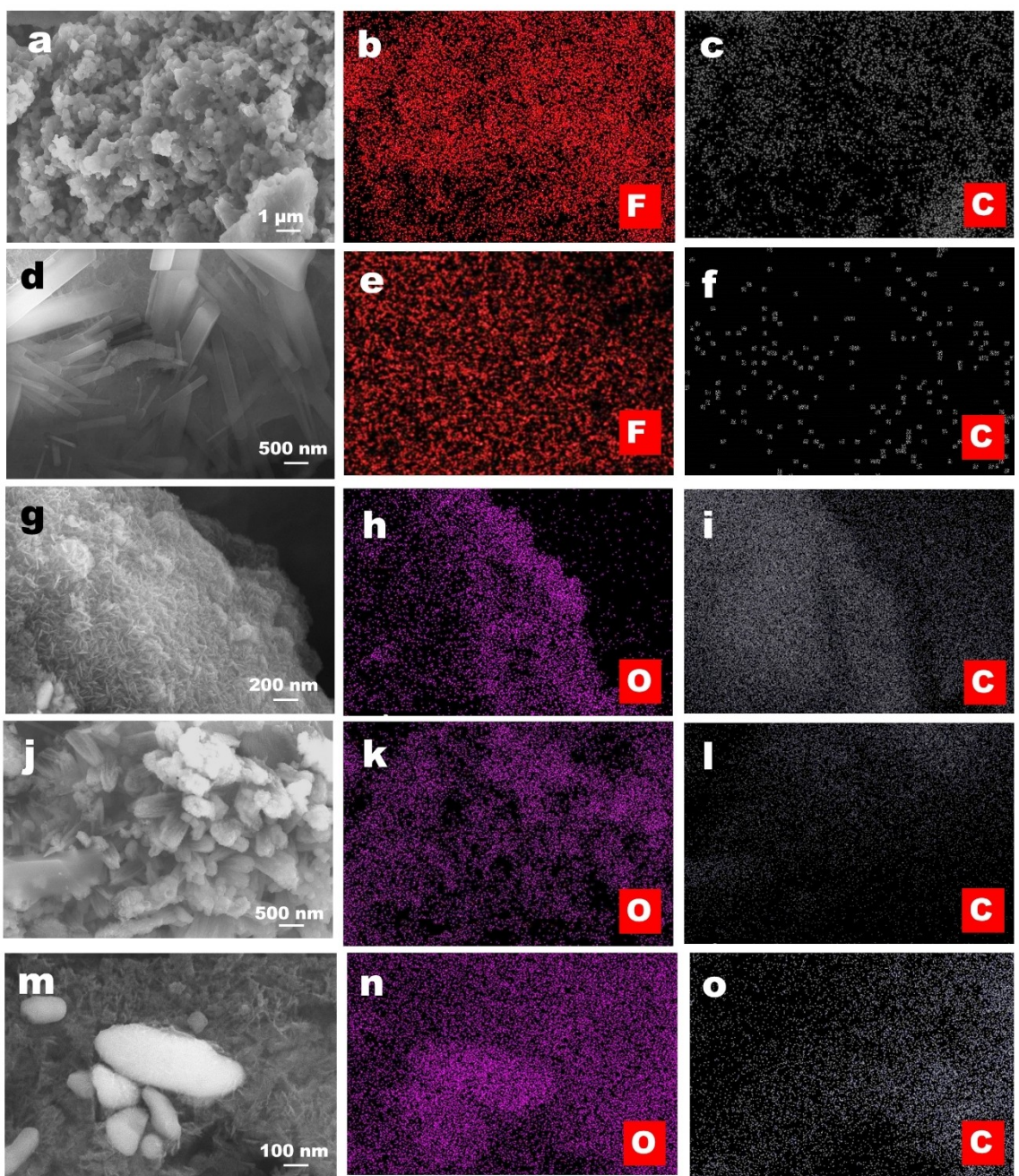


Figure 6. Morphology of SEI layer after 1st lithiation and corresponding EDX elemental mapping: a–c) granular; d–f) rod-like; g–i) needle-like; j–l) corn-like, and m–o) bead-like structures.

2.6. Electrochemical Impedance Analysis

The electrochemical impedance spectroscopy (EIS) spectrum of the lithium-ion cell was recorded in a wide frequency range (100 kHz to 50 mHz) at different stages during electrochemical cycling. The 1st cycle EIS spectra at different lithiation and delithiation potentials are shown in Figure 8a. The change in the EIS spectrum profile during the lithiation and delithiation of the graphite indicates that lithium-ion rate kinetics varies.^[28] In the EIS spectrum, the high and middle-frequency regions (100 kHz to 10 Hz) are attributed to SEI layer growth, while the

low-frequency region (10 Hz to 50 mHz) corresponds to the lithium-ion diffusion rate kinetics.^[1,4] In our previous work, the mosaic SEI layer formation and its influence on the lithium-ion rate kinetics were studied as a function of discharge voltage.^[4] The SEI layer resistance (R_{SEI}), Ohmic resistance (R_0), and the charge transfer resistance (R_{ct}) were measured from the Nyquist plot by fitting with an electrochemical equivalent circuit (EEC).^[4,6] During 1st lithiation, the R_{SEI} increases with decreasing cell voltage (Figure 8a). This could be due to the continuous formation of the SEI layer.^[4]

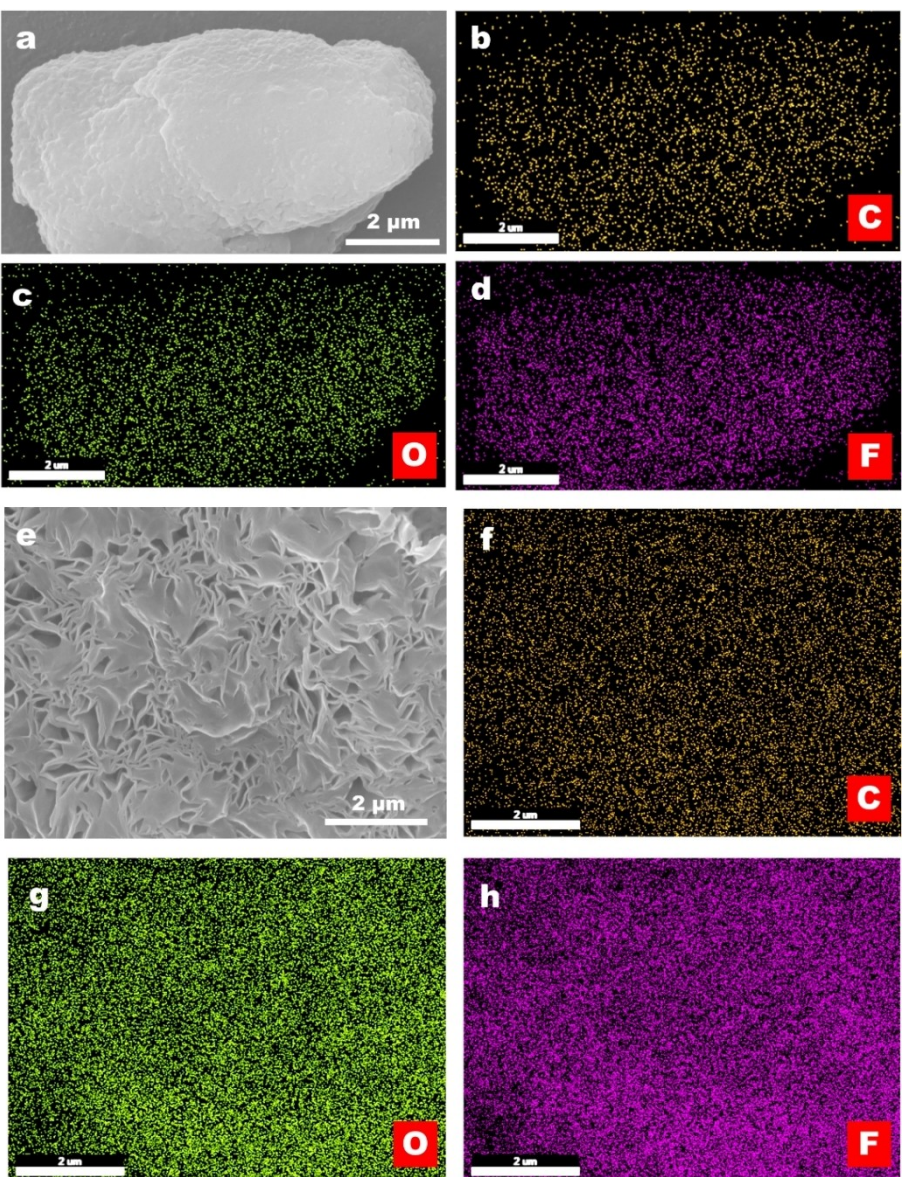


Figure 7. a) Graphite particle uniformly covered with SEI layer after 20th lithiation and b-d) corresponding EDX mapping; e) porous morphology of outer SEI layer, and f-h) corresponding EDX mapping.

Whereas the R_{ct} decreases with decreasing cell voltage which facilitates the lithium-ion diffusion. During subsequent delithiation, the R_{SEI} remained nearly invariant, While the R_{CT} decreased considerably at the complete delithiation (2 V). The EIS spectra were acquired after different lithiation and delithiation cycles (8b, d) to understand further the loss of reversible lithium ions during initial cycles at high 0.5 C (Figure 1c). A small variation in the R_{SEI} was observed during cycling due to the decomposition of the entrapped electrolyte, and after 20th lithiation, the R_{SEI} was found to be higher than that after 1st lithiation (Figure 8c). In contrast, the R_{CT} after the 20th lithiation was found to be lower than that of the 1st delithiation. This signifies that during cycling at a 0.5 C rate, the densification of the SEI has occurred, leading to the formation of an electrically insulating stable SEI layer after 10 cycles. Irrespective of the delithiation cycles, the cell resistance (R_0)

was found to be unchanged (Figure 8e), which ensured stable electrochemical cycling. The $R_{SEI} + R_{CT}$ ($R_{SEI} \gg R_{CT}$) was gradually increasing over the cycles due to the densification of the SEI. After 10 cycles, the $R_{SEI} + R_{CT}$ increased significantly due to a stable SEI layer on the graphite surface.

3. Conclusion

In summary, we have investigated the mosaic SEI layer's growth and stability on graphite anode. After 1st lithiation, a uniform SEI layer with a thickness of 150 nm was formed on the graphite particles. Although the densification of the SEI layer was observed after cycling (20th lithiation), the SEI layer thickness was almost unchanged. The XPS depth profile studies were conducted to appreciate the structure of the mosaic SEI

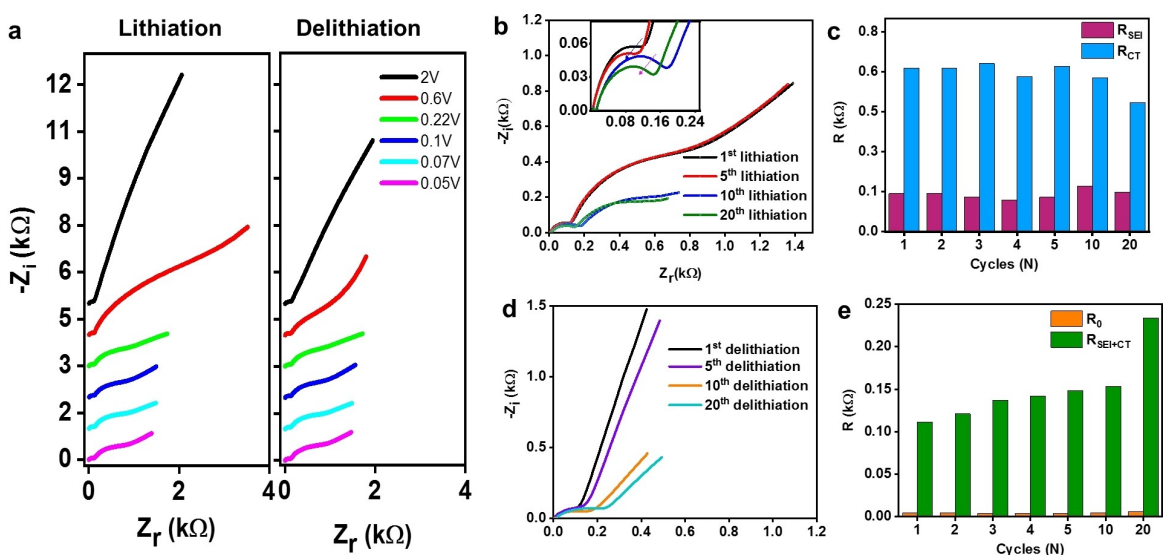


Figure 8. EIS spectra of graphite anode. a) The EIS spectrum obtained at different lithiation and delithiation voltages in the 1st cycle; b) EIS spectra after different lithiation cycles, and inset magnified image of the EIS spectra at high-frequency region, c) corresponding R_{SEI} and R_{CT} at various cycle numbers; d) EIS spectra after different delithiation cycles; e) corresponding R_0 and $R_{SEI} + R_{CT}$ at various cycle numbers.

layer. The relatively compact inorganic compound-rich outer mosaic SEI layer is critical for preventing the electrolyte decomposition after 1st cycle and ceasing the mosaic SEI layer growth in subsequent cycles. After cycling, the relative amount of organic compounds increased in the outer part of the mosaic SEI layer. This could be attributed to an increase in current density, favouring the one-electron reduction reaction for organic compounds. A “sponge model” for the SEI densification process is proposed to explain the densification of the SEI layer where the trapped electrolyte inside the pores of the SEI layer further undergoes decomposition leading to the formation of more SEI compounds. The SEI layer formed after 1st lithiation showed various morphological features corresponding to various SEI compounds. After 20th lithiation, a porous outer SEI layer with uniform distribution of organic and inorganic compounds was observed on the graphite anode. Hence, the chemical composition of the mosaic SEI layer determines the SEI layer’s stability during subsequent cycling, which minimizes the loss of reversible lithium ions and extends the cycle life of a LIB.

Acknowledgments

The authors would like to acknowledge the financial support from the Technical Research Centre (TRC), Department of Science & Technology (TRC project: AI/1/65/ARCI/2014), Government of India for the completion of this work. The authors also thank Late Dr. G. Padmanabham, Former Director, ARCI, for his constant encouragement and support for this work.

Conflict of Interest

The authors declare no conflict of interest.

Keywords: cycle life · electrochemistry · lithium-ion battery · reaction mechanisms · solid electrolyte interface

- [1] S. Sahu, V. Rikka, P. Haridoss, A. Chatterjee, R. Gopalan, R. Prakash, *Adv. Energy Mater.* **2020**, *10*, 2001627.
- [2] J. Pender, G. Jha, D. Youn, J. Ziegler, I. Andoni, E. Choi, A. Heller, B. Dunn, P. Weiss, R. Penner et al., *ACS Nano* **2020**, *14*, 1243–1295.
- [3] J. Ming, Z. Cao, W. Wahyudi, M. Li, P. Kumar, Y. Wu, J. Hwang, M. Hedhili, L. Cavallo, Y. Sun et al., *ACS Energy Lett.* **2018**, *3*, 335–340.
- [4] V. Rikka, S. Sahu, A. Chatterjee, P. Satyam, R. Prakash, M. Rao, R. Gopalan, G. Sundararajan, *J. Phys. Chem. C* **2018**, *122*, 28717–28726.
- [5] S. An, J. Li, C. Daniel, D. Mohanty, S. Nagpure, D. Wood, *Carbon* **2016**, *105*, 52–76.
- [6] W. Huang, P. Attia, H. Wang, S. Renfrew, N. Jin, S. Das, Z. Zhang, D. Boyle, Y. Li, M. Bazant et al., *Nano Lett.* **2019**, *19*, 5140–5148.
- [7] X. Yu, A. Manthiram, *Energy Environ. Sci.* **2018**, *11*, 527–543.
- [8] C. Yan, Y. X. Yao, W. L. Cai, L. Xu, S. Kaskel, H. S. Park, J. Q. Huang, *J. Energy Chem.* **2020**, *49*, 335–338.
- [9] I. Weber, B. Wang, C. Bodirsky, M. Chakraborty, M. Wachtler, T. Diermant, J. Schnait, R. Jürgen Behm, *ChemElectroChem* **2020**, *7*, 4794–4809.
- [10] L. L. Jiang, C. Yan, Y. X. Yao, W. Cai, J. Q. Huang, Q. Zhang, *Angew. Chem. Int. Ed.* **2021**, *60*, 3402–3406; *Angew. Chem.* **2021**, *133*, 3444–3448.
- [11] H. Sun, A. Dolocan, J. Weeks, R. Rodriguez, A. Heller, C. Mullins, *J. Mater. Chem. A* **2019**, *7*, 17782–17789.
- [12] S. Ahamed, A. Gupta, *Electrochim. Acta* **2020**, *341*, 136015.
- [13] Y. Ein-Eli, *Electrochim. Solid-State Lett.* **1999**, *2*, 212.
- [14] E. Peled, D. Golodnitsky, G. Ardel, *J. Electrochem. Soc.* **1997**, *144*, L208–L210.
- [15] K. Edström, M. Herstedt, D. Abraham, *J. Power Sources* **2006**, *153*, 380–384.
- [16] H. Shin, J. Park, S. Han, A. Sastry, W. Lu, *J. Power Sources* **2015**, *277*, 169–179.
- [17] J. Yan, B. Xia, Y. Su, X. Zhou, J. Zhang, X. Zhang, *Electrochim. Acta* **2008**, *53*, 7069–7078.
- [18] S. Nadimpalli, V. Sethuraman, S. Dalavi, B. Lucht, M. Chon, V. Shenoy, P. Guduru, *J. Power Sources* **2012**, *215*, 145–151.

- [19] F. Li, J. He, J. Liu, M. Wu, Y. Hou, H. Wang, S. Qi, Q. Liu, J. Hu, J. Ma, *Angew. Chem. Int. Ed.* **2020**, *60*, 6600–6608.
- [20] X. Li, J. Liu, J. He, H. Wang, S. Qi, D. Wu, J. Huang, F. Li, W. Hu, J. Ma, *Adv. Funct. Mater.* **2021**, *20*, 2104395.
- [21] S. Qi, H. Wang, J. He, J. Liu, C. Cui, M. Wu, F. Li, Y. Feng, J. Ma, *Sci. Bull.* **2021**, *66*, 685–693.
- [22] S. Schweidler, L. de Biasi, A. Schiele, P. Hartmann, T. Brezesinski, J. Janek, *J. Phys. Chem. C* **2018**, *122*, 8829–8835.
- [23] Q. Shi, S. Heng, Q. Qu, T. Gao, W. Liu, L. Hang, H. Zheng, *J. Mater. Chem. A* **2017**, *5*, 10885–10894.
- [24] T. Zhu, Q. Hu, G. Yan, J. Wang, Z. Wang, H. Guo, X. Li, W. Peng, *Energy Technol.* **2019**, *7*, 1900273.
- [25] F. Soto, Y. Ma, J. Martinez de la Hoz, J. Seminario, P. Balbuena, *Chem. Mater.* **2015**, *27*, 7990–8000.
- [26] J. Henschel, C. Peschel, S. Klein, F. Horsthemke, M. Winter, S. Nowak, *Angew. Chem. Int. Ed.* **2020**, *59*, 6128–6137; *Angew. Chem.* **2020**, *132*, 6184–6193.
- [27] I. Shkrob, Y. Zhu, T. Marin, D. Abraham, *J. Phys. Chem. C* **2013**, *117*, 19255–19269.
- [28] M. Steinhauer, S. Rissee, N. Wagner, K. Friedrich, *Electrochim. Acta* **2017**, *228*, 652–658.

Manuscript received: June 7, 2021
Revised manuscript received: July 5, 2021
Accepted manuscript online: July 6, 2021
Version of record online: August 4, 2021